

Supporting information

Mildly Regulated Intrinsic Faradaic Layer at Oxide/Water Interface for Improved Photoelectrochemical Performance

Ziyu Yin^a, Xiangtian Chen^a, Cheng Wang^b, Zijing Guo^c, Xinglong Wu^c, Zongyan Zhao^d, Yingfang Yao^{*.b}, Wenjun Luo^{*.b}, Zhigang Zou^{a,b,e,f}

^aEco-materials and Renewable Energy Research Center (ERERC), Jiangsu Key Laboratory for Nano Technology, National Laboratory of Solid State Microstructures and Department of Physics, Nanjing University, Nanjing 210093, China

^bEco-materials and Renewable Energy Research Center (ERERC), College of Engineering and Applied Sciences, Nanjing University, Nanjing 210093, China

^cNational Laboratory of Solid State Microstructures and Department of Physics, Nanjing University, Nanjing 210093, China

^dFaculty of Materials Science and Engineering, Kunming University of Science and Technology, Kunming 650093, China

^eSchool of Science and Engineering, The Chinese University of Hong Kong, Shenzhen, 2001 Longxiang Blvd., Longgang District, Shenzhen 518172, China

^fMacau Institute of Systems Engineering, Macau University of Science and Technology, Macau 999078, China

*Email: yaoyingfang@nju.edu.cn; wjluo@nju.edu.cn;

Preparation of the TiO₂ thin films

TiO₂ films were prepared by hydrothermal method.¹ Typically, 15 mL deionized water and 15 mL HCl (36%-38%) were mixed to obtain clear solution. And then, 0.45 mL titanium butoxide was added with stirring. The precursor solution was removed into

a 25 mL teflon-lined steel autoclave. Some FTO glass was immersed in the solution as substrate. The hydrothermal process maintained at 150 °C for 9 hours. The deposited films were washed and calcined in a muffle furnace at 450 °C for 1 hour in air.

Preparation of the Fe₂O₃ thin films

The Ti doped hematite films were also prepared by similar hydrothermal method.² Typically, 7.5 mmol FeCl₃·6H₂O and 50 μL TiCl₃ were added into 100 mL deionized water. Then 0.6 mL HCl (36%-38%) were added into the solution to adjust the pH. The solution was transferred into the 100 mL teflon-lined steel autoclave and some FTO glass was immersed in the solution as substrate. The hydrothermal process maintained at 100 °C for 4 hours. The deposited FeOOH films were calcined in the muffle furnace at 675 °C for 15min in air and taken out at 575 °C.

Heat-treatment of the oxide films

The obtained TiO₂ and Fe₂O₃ thin films were calcined in the muffle furnace at 100 °C, 200 °C and 400 °C in the air, respectively.

Characterization of samples

The crystal structures of the samples are characterized by X-ray diffraction (XRD smartlab, 9 kW). The morphologies of the samples were investigated by scanning electron microscope (SEM Nano Nova S230) with an accelerating voltage of 15 kV. Raman was examined by Horiba T64000 @ 514 nm. The photoluminescence spectra (PL) of TiO₂ samples were collected by a Renishaw InVia Raman Micro-PL system with a 375 nm He-Cd laser. The X-ray photoelectron spectroscopy (XPS) were performed on a K-Alpha instrument operating with an Al K α X-ray source. The binding energy of the C1s peak at 284.6eV was used as an internal standard to calibrate the data. The optical absorption spectra of the samples were characterized by GG49-Lam950. The contact angles for water were measured using a contact angle goniometer (JGW-360A, Chenghui).

Photoelectrochemical measurement

The photoelectrochemical properties of the films were investigated in a three-electrode cell using an electrochemical analyzer (CHI 760e, Shanghai Chenhua) under AM 1.5

sunlight simulator illumination. The prepared films were used as the working electrode, and a Pt foil and a saturated Ag/AgCl electrode as a counter and a reference electrode, respectively. The electrolytes were 1 M KOH (pH~13.6), 0.1 M HClO₄ (pH~1). Moreover, 1 M KOH aqueous solution with 0.5 M Na₂SO₃ as sacrificial agent was also used as electrolyte. The RHE potential was calculated from the following formula: $V_{\text{RHE}} = V_{\text{Ag/AgCl}} + 0.059 \cdot \text{pH} + 0.197$. The incident photon to current efficiency (IPCE) spectra was measured under monochromatic light irradiation, provided by the AM 1.5 sunlight simulator equipped with band pass filters. The light intensity was obtained with a photometer (Newport, 1919-R).

Computational method and models

In the present study, all of density functional theory (DFT) calculations have been carried out by using Cambridge Serial Total Energy Package (CASTEP) codes, employing the ultrasoft pseudopotential.³ Exchange and correlation effects were described by the revised Perdew-Burke-Ernzerhof for solid (PBEsol) of generalized gradient approximation (GGA).⁴ An energy cutoff of 340 eV has been used for expanding the Kohn-Sham wave functions. The minimization algorithm has been chosen Broyden-Fletcher-Goldfarb-Shanno (BFGS) scheme.⁵ The K-points grid sampling of Monkhorst-Pack scheme was set as 2×2×1 in the irreducible Brillouin zone, and the fast Fourier transform grid was set as 64×72×192. To get accurate results, we optimized atomic coordinates, which obtained by minimizing the total energy and atomic forces. This was done by performing an iterative process in which the coordinates of the atoms are adjusted so that the total energy of the structure is minimized. The relaxation run was considered converged when the force on the atomic nuclei was less than 0.03 eV/Å, the stress on the atomic nuclei was less than 0.05 GPa, the displacement of the nuclei was less than 1×10⁻³ Å, and the energy change per atom was less than 1×10⁻⁵ eV. In order to improve accuracy of calculated adsorption energies for water on TiO₂ surfaces, the dipole corrections were utilized for all models, which can be essential in eliminating nonphysical electrostatic interaction between periodic

images.⁶

The rutile TiO₂ (110) surface is simulated by a (4×2) (i.e. 11.788 Å×13.026 Å) periodic slab of 5 O-Ti-O trilayers (80 TiO₂ units, 240 atoms). The slab models are separated by a 20-Å-thick vacuum layer. The lengths of these models are larger than 10 Å, which are enough to avoid the self-interaction effects of the periodic boundary conditions. The bottom two trilayers of the slab are fixed to mimic the bulk effects.

Water molecule was placed near the surface, and then optimized to get the most stable molecular adsorption state of water on these surfaces. Near the position of molecular adsorption position, the possible dissociative adsorption configurations were all considered. Because the partial decomposition (H₂O→H+OH) of water is easier than the complete decomposition (H₂O→2H+O), and the surface hydroxyl radical is more critical for the photocatalysis. So, we only considered partial decomposition of water in this article. Compared the adsorption energy of water on different surface locations, we get the most stable molecular adsorption state or dissociative adsorption state of water on these surfaces, i.e. the minimum adsorption states. Subsequently, these two states were respectively set as the initial state (reactant) and the final state (product). Based on these configurations, the transition state on the minimum reaction energy pathway was identified, using the complete linear synchronous transit (LST) and quadratic synchronous transit (QST) search methods followed by transition-state confirmation through the nudged elastic band (NEB) method.⁷⁻¹³ On the basis of the calculated adsorption energy of these states, we analyzed the reaction activity and energy for the decomposition reaction of water on rutile TiO₂ surfaces.

Using the above calculation method, we first optimized the bulk crystal structure of rutile TiO₂, and obtained the following lattice constants: a = b = 4.6054 Å, c = 2.9471 Å. This calculation results are well consistent with the experimental measurements:¹⁴ a = b = 4.5931 Å, c = 2.9589 Å. Then, we optimized the structure of clean TiO₂ surface using above calculation method, obtaining the surface configuration that is well consistent with previous reports.¹⁵ These calculated results indicate that the calculation models and method in the present study are reasonable.

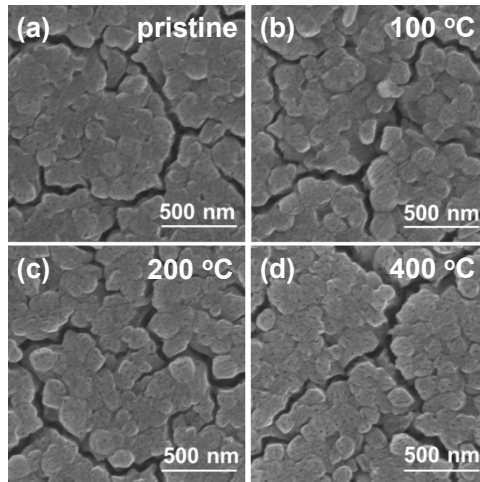


Figure S1. SEM images of Fe_2O_3 before (a) and after the heat-treatment in air at 100 °C (b), 200 °C (c) and 400 °C (d).

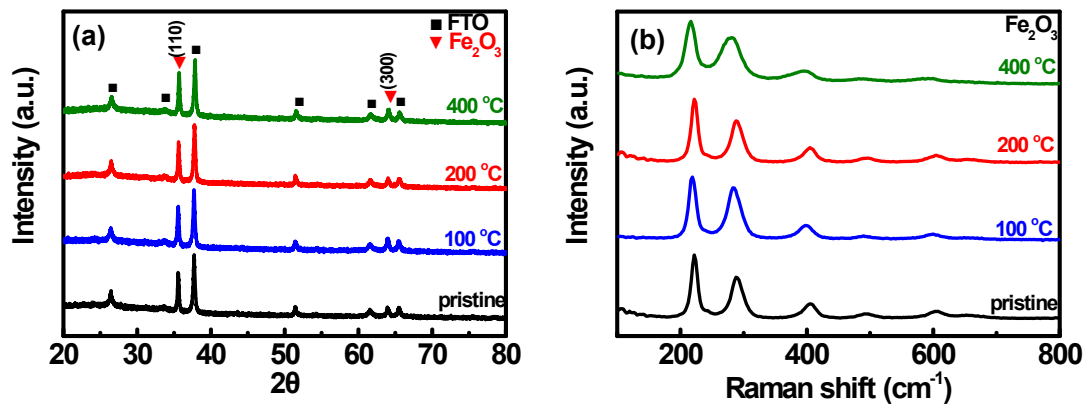


Figure S2. X-ray diffraction (XRD) patterns (a) and Raman spectroscopy XRD (b) Fe_2O_3 before and after the heat-treatment in air at different temperatures.

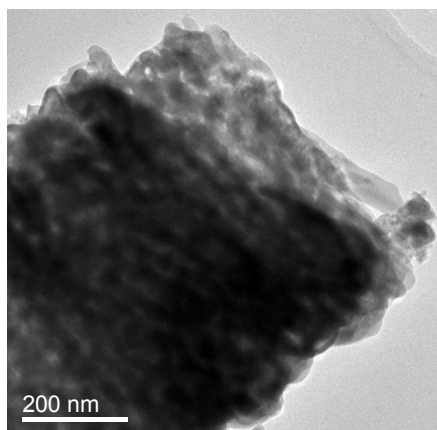


Figure S3. Transmission electron microscope (TEM) images of Fe₂O₃ sample before the heat-treatment.

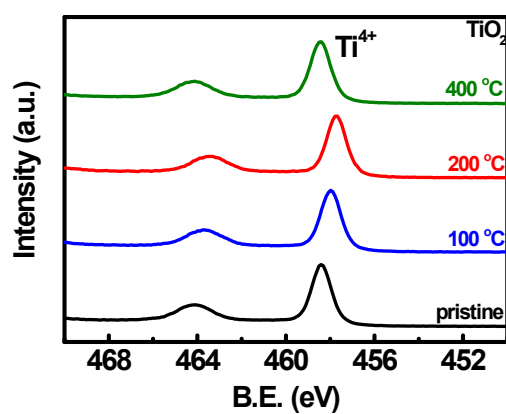


Figure S4. X-ray photoelectron spectroscopy (XPS) of Ti 2p of the surface on the TiO₂ samples before and after the heat-treatment at different temperatures.

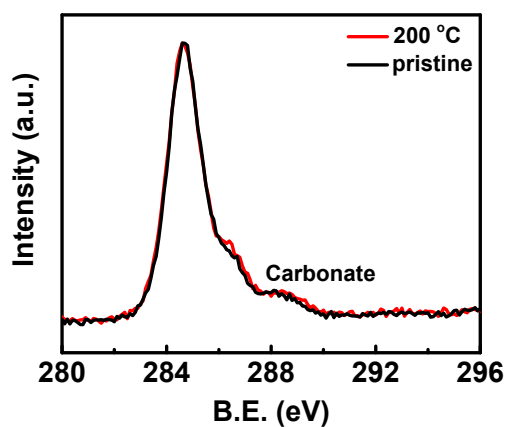


Figure S5. X-ray photoelectron spectroscopy (XPS) of C 1s in the TiO₂ before and after heat-treatment at 200 °C.

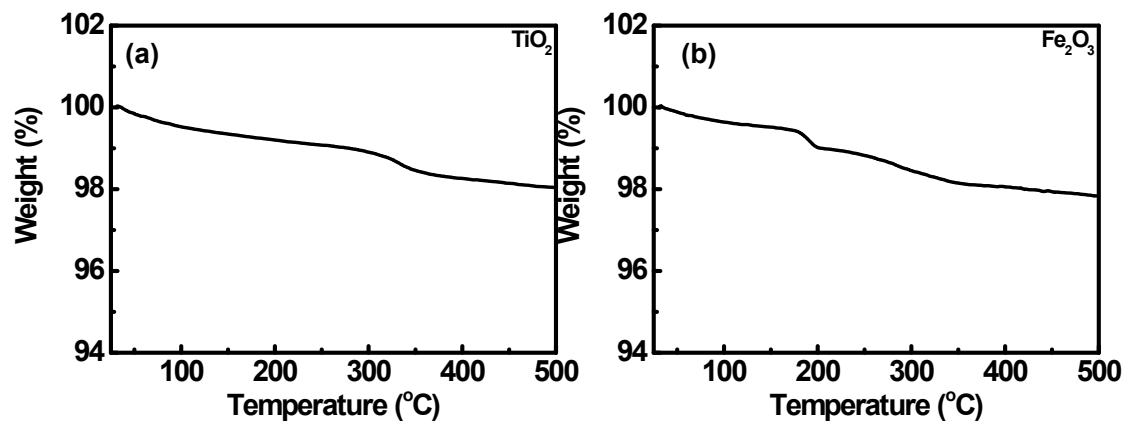


Figure S6. Thermogravimetric analysis (TGA) of TiO₂ (a) and Fe₂O₃ (b) samples before heat-treatment which had been scratched from FTO substrates, respectively.

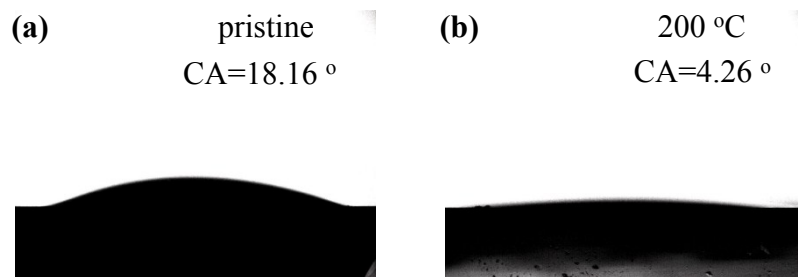


Figure S7. The contact angles of TiO₂ before (a) and after heat-treatment at 200 °C (b).

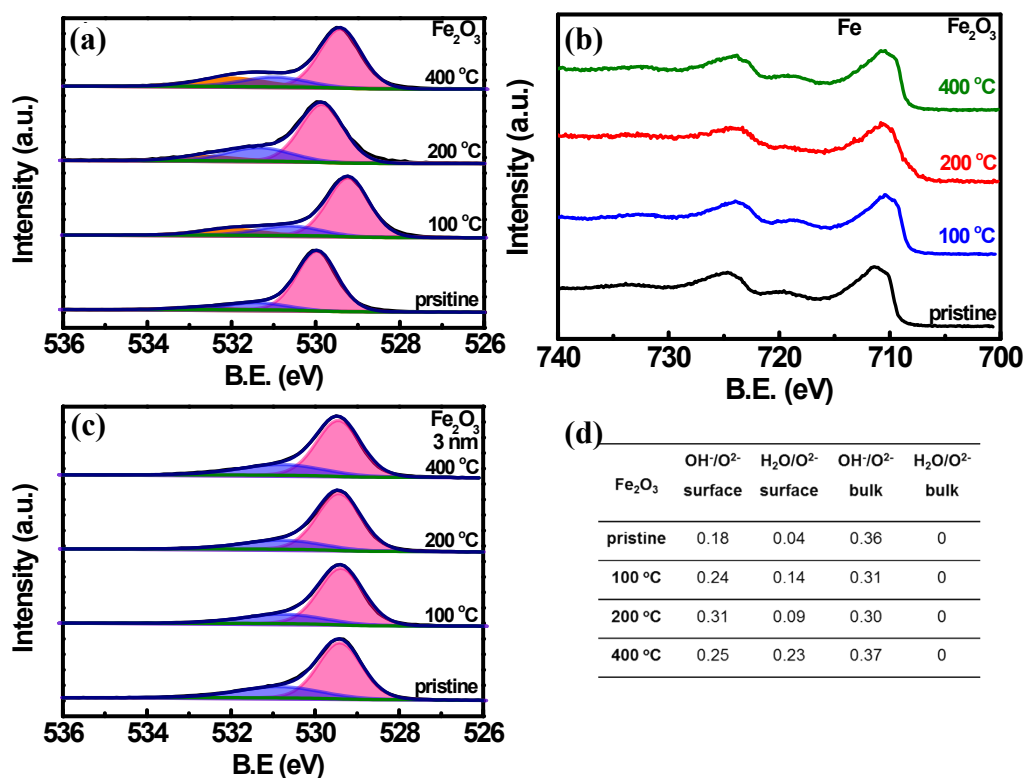


Figure S8. X-ray photoelectron spectroscopy (XPS) of O 1s of the surface (a) and the bulk (3 nm depth) (c) of Fe₂O₃ before and after heat-treatment at different temperatures; XPS of Fe 2p of the surface (b) of Fe₂O₃ samples before and after the heat-treatment at different temperatures; A table of the XPS ratio of lattice OH⁻ and chemically adsorbed H₂O to lattice O²⁻ on the surface and in the bulk (3 nm depth) of Fe₂O₃ (d).

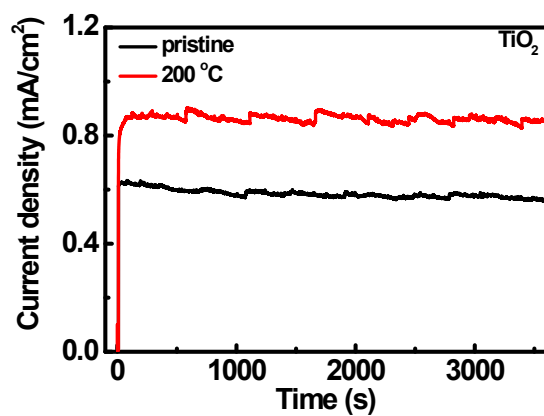


Figure S9. I-t curves of TiO₂ before and after the heat-treatment at 200 °C in 1M KOH.

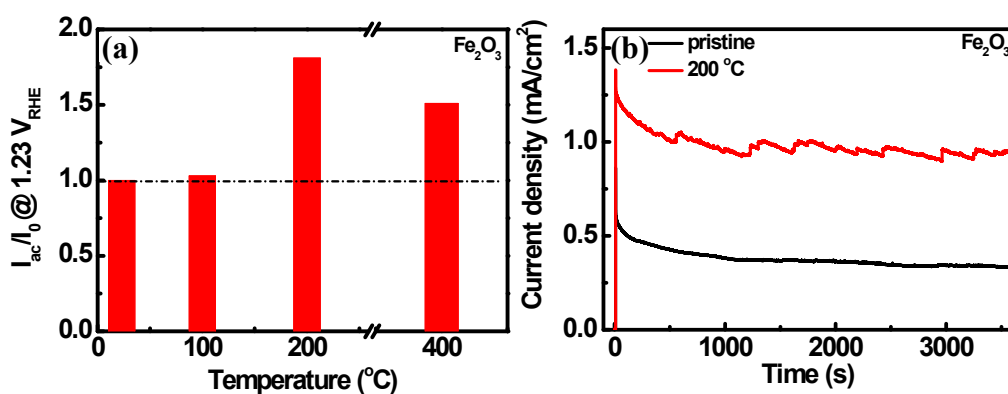


Figure S10. Photocurrent ratio of Fe_2O_3 at different heat-treatment temperatures to a pristine sample at $1.23 V_{RHE}$ (a), I_{ac} is the photocurrent of the samples at heat-treated temperatures and I_0 is the photocurrent of a pristine sample; I-t curves of Fe_2O_3 before and after the heat-treatment at $200^{\circ}C$ in 1M KOH;

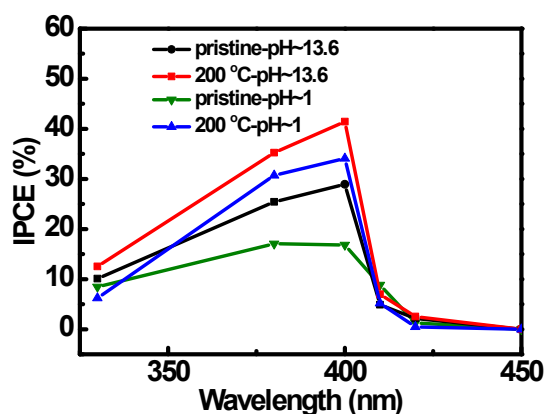


Figure S11. IPCE spectra of the TiO_2 before and after $200^{\circ}C$ heat-treatment collected at $1.23 V$ vs. RHE in different pH electrolytes, 1 M KOH (pH ~ 13.6) and 0.1 M $HClO_4$ (pH ~ 1), respectively.

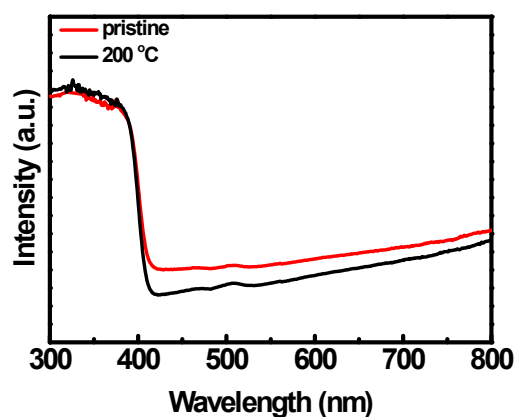


Figure S12. UV-Vis absorption spectra of TiO₂ before and after the heat-treatment at 200 °C.

References

- (1) X. Xia, J. Luo, Z. Zeng, C. Guan, Y. Zhang, J. Tu, H. Zhang, H. Fan, *Sci. Rep.*, 2012, **2**, 981.
- (2) T. Wang, W. Luo, X. Wen, Z. Zou, W. Huang, *ChemNanoMat*, 2016, **2**, 652-655.
- (3) S. J. Clark, M. D. Segall, C. J. Pickard, P. J. Hasnip, M. J. Probert, K. Refson, M. C. Payne, *Z Kristallogr.*, 2005, **220**, 567-570.
- (4) J. P. Perdew, A. Ruzsinszky, G. I. Csonka, O. A. Vydrov, G. E. Scuseria, L. A. Constantin, X. Zhou, K. Burke, *Phys. Rev. Lett.*, 2008, **100**, 136406.
- (5) B. G. Pfrommer, M. Côté, S. G. Louie, M. L. Cohen, *J. Comput. Phys.*, 1997, **131**, 233-240.
- (6) J. Neugebauer, M. Scheffler, *Phys. Rev. B*, 1992, **46**, 16067-16080.
- (7) T. A. Halgren, W. N. Lipscomb, *Chem. Phys. Lett.*, 1977, **49**, 225-232.
- (8) W. Gao, M. Zhao, Q. Jiang, *J. Phys. Chem. C*, 2007, **111**, 4042-4046.
- (9) A. Simperler, A. Kornherr, R. Chopra, W. Jones, G. Zifferer, *Phys. Chem. Chem. Phys.*, 2007, **9**, 3999-4006.

- (10) N. Govind, M. Petersen, G. Fitzgerald, D. King-Smith, J. Andzelm, *Comp. Mater. Sci.*, 2003, **28**, 250-258.
- (11) M. Sun, A. E. Nelson, J. Adjaye, *J. Catal.*, 2005, **233**, 411-421.
- (12) M. Sun, A. E. Nelson, J. Adjaye, *J. Catal.*, 2005, **231**, 223-231.
- (13) G. Henkelman, H. Jonsson, *J. Chem. Phys.*, 2000, **113**, 9978-9985.
- (14) J. K. Burdett, T. Hughbanks, G. J. Miller, J. W. Richardson, J. V. Smith, *J. Am. Chem. Soc.*, 1987, **109**, 3639-3646.
- (15) M. Ramamoorthy, D. Vanderbilt, R. D. King-Smith, *Phys. Rev. B*, 1994, **49**, 16721.